AIAA 80-0076R

Flow Measurements in a Model Swirl Combustor

Bach T. Vu* and F. C. Gouldin†
Cornell University, Ithaca, N. Y.

Measurements in a model combustor composed of two confined coaxial swirling jets under noncombusting conditions are presented. Mean flow results are obtained for five different flow conditions to determine the effect of outer swirl on the recirculation zone. As the outer swirl magnitude is first decreased from maximum counterswirl to zero and then increased to give coswirl conditions, the size of and the reverse flow velocity in the recirculation zone diminish. Detailed time mean and fluctuating flow measurements are obtained for a coswirl and a counterswirl condition with a directional pitot probe and hot-wire anenometer. For these cases, a recirculation zone occurs only with counterswirl. The recirculation zone is a single-cell torroidal vortex having low swirl velocity. Axial development of turbulence levels, energy dissipation rates, and length scales are described for the two flow conditions. Spectral analysis reveals periodic oscillations in both flows. The oscillations originate from the inner jet, and up to four harmonics are observed. The fundamental frequencies are comparable to the rotational frequencies of the inner jet flows.

Nomenclature

D_i = inner diameter of inner tube
D_o = diameter of test section
E = power spectrum
f = frequency
f_d = dissipation frequency obtained by assuming Taylor's hypothesis
k = wave number
k_d = dissipation wave number
ℓ = turbulence macroscale
P = static pressure
P_w = static pressure at test section wall
P_ℓ = centerline static pressure
P_w^i = P_w at the inlet axial station
P_ℓ^i = P_ℓ at the inlet axial station
q' = fluctuating velocity component parallel to the mean velocity
q = rms value of q'
Q = mean velocity magnitude
R = radial distance
R_i = inner radius of inner tube
R_o = radius of test section
S = swirl parameter
S_i = S for inner jet
S_o = S for outer jet
t = time
T = temperature
U = mean axial velocity
$(U_i)_{av}$ = bulk average velocity of inner jet
$(U_o)_{av}$ = bulk average velocity of outer jet
U_{BF} = magnitude of back flow velocity
W = mean tangential velocity
Z = axial distance
ϵ = energy dissipation rate
η = Kolmogorov length scale
λ = Taylor length scale
ν = kinematic viscosity
ρ = density
ψ = stream function

Presented as Paper 80-0076 at the AIAA 18th Aerospace Sciences Meeting, Pasadena, Calif., Jan. 14-16, 1980; submitted Jan. 26, 1981; revision received Oct. 5, 1981.

*1980 Graduate Research Assistant; presently Associate Scientist, Avco Everett Research Laboratory, Inc., Everett, Mass.

†Associate Professor, Sibley School of Mechanical and Aerospace Engineering. Member AIAA.

I. Introduction

An important application of swirling flow lies in its use to provide flame stabilization and improved mixing in many combustion chambers. In the study of swirling flows, the term vortex breakdown refers to the formation of a free stagnation point or recirculation zone on the axis of flows with significant streamwise vorticity.[1,2] The swirl-induced recirculation zones observed in swirl combustors are felt to be examples of vortex breakdown.

In order to achieve enhanced flame stabilization and better control of mixing processes, multiple coaxial swirling streams can be introduced in swirl combustors. A series of experiments have been carried out on a model combustor that uses two coaxial swirling jets.[3-5] It is found that fluid mechanical phenomena play an important role in determining the operation of the combustor.

In this paper we present the results of a set of experiments on a model swirl combustor under noncombusting conditions. Flow measurements with a pitot probe and hot-wire anemometer are carried out in a flow apparatus of a geometrical configuration similar to the model, two-stream, swirl combustor mentioned above. As shown in Fig. 1, the flow consists of two coaxial swirling streams where the outer swirl can be adjusted from coswirl (streams rotating in the same direction) to counterswirl conditions. The objectives are to achieve a better understanding of the complex phenomena associated with swirling flow and to provide data for developing and evaluating numerical flow prediction models.

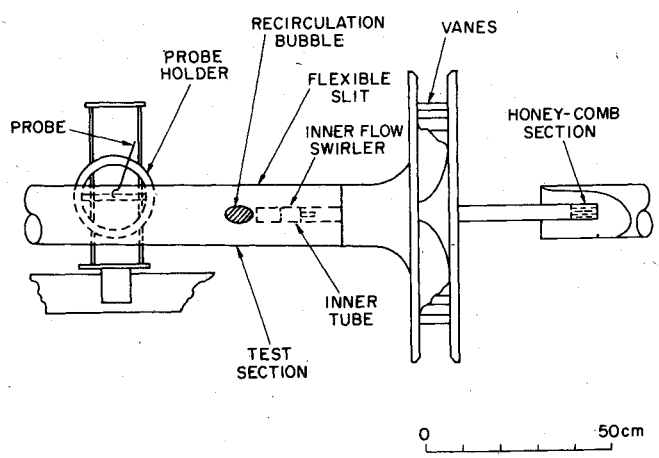

Fig. 1 Schematic of apparatus.

In a first group of experiments, mean flow measurements are made to determine the influence of outer swirl on the size of the recirculation zone and on the magnitude of the reverse flow velocity. In a second group of experiments detailed measurements of the mean flow and turbulence properties for one coswirl and one counterswirl flow condition are undertaken. Nonrandom, periodic fluctuations are also of interest; their study is undertaken by spectral analysis.

II. Experiment

Flow Apparatus

The overall flow apparatus consists of a test section, two swirl generators, two blowers, and two plenum chambers. The test section, Fig. 1, is a clear acrylic pipe 14.5 cm in diameter. In the first group of experiments, the inner jet issues into the test section from a brass tube with an outer diameter of 3.86 cm and an inner diameter of 3.43 cm. In the second group of experiments, the inner jet flows from a thin stainless steel tube with an outer diameter of 3.81 cm and an inner diameter of 3.72 cm. The inner and outer tubes are aligned to be concentric within ± 0.15 cm and parallel within ± 0.2 deg. Airflows are generated by two blowers: a small (3 hp) blower that forces air from a plenum through the inner tube and a large (25 hp) one which draws air from the test section through a diffuser and plenum intended to damp out fluctuations created by the blower. For hot-wire measurements air filters are used in both inner and outer flows to avoid dust collection on the hot wire. Flow rates are controlled by adjustable vanes and bleed nozzles.

Swirl for the inner jet is generated by a small axial flow swirl generator with fixed vanes, which is located in the inner tube several diameters upstream of the inner jet exit (15.2 cm for the first group of experiments and 12.2 cm for the second group of experiments). The generator consists of 12 equally spaced vanes placed in the annular volume between a center tube (1.27 cm o.d.) and an outer casing (3.56 cm i.d.). These vanes are cut from long aluminum strips ($3.78 \times 1.14 \times 0.05$ cm) with the upstream parts parallel to the axis of the flow, and the downstream ends bent 68.5 deg from the axial direction. Such a vane configuration can smoothly guide the flow and impart swirl to it. Swirl for the outer jet is generated by an assembly of 24 adjustable vanes. Air is drawn radially inward through the vane assembly and deflected into the test section by a turning channel. The vane assembly consists of two annular plates supporting 24 equally spaced vanes between them. The 24 streamlined vanes are symmetrically positioned around one of the plates with their pivoting axes on a circle 55.88 cm in diameter. A chain and sprocket mechanism collectively rotates the vanes so that they all make the same, adjustable angle with the radial flow direction. This angle is continuously variable between -80 and $+80$ deg, and its value can be read on a protractor accurately to ± 0.05 deg. In the outer flow, the boundary layers on the outer and inner walls are tripped to insure turbulent flow. Tangential velocity measurements by a five-hole pitot probe at the test section inlet show solid body rotation in the inner jet core away from the boundary layer and a free vortex in the outer flow outside the wall boundary layers. A free vortex is the consequence of tangential momentum conservation.

Flow Parameters

For the first set of experiments, the axial velocity averaged across the entire cross section is about 30 m/s, which corresponds to a Reynolds number based on a diameter of about 250,000. During the second set, where hot-wire anemometry is used, the average axial velocity is lowered (so that the measured velocities fall within the hot-wire calibration range) to approximately 20 m/s, corresponding to a Reynolds number of 170,000. At these high flow rates, the flow features are expected to be Reynolds number independent. Pitot probe measurements and hot-wire measurements for coswirl at $Re = 170{,}000$ and at $Re = 250{,}000$ (all flow parameters except the Reynolds number are constant) show that there is almost no difference between the observed flow features at the two Reynolds numbers. Thus the results of these experiments can be considered typical of high Reynolds number flows in general.

The swirl parameter, which is closely related to the swirl number, is defined at the initial axial station (exit of the inner jet at the test section inlet) as

$$S = \frac{\text{axial flux of angular momentum}}{(\text{axial flux of linear momentum})R} \tag{1}$$

where $R = R_i$ for the inner jet and $R = R_o$ for the outer jet. S values for inner and outer flows are obtained by integration of flow profiles measured at the test section inlet.

Instrumentation

Mean flow measurements are made with a directional pitot probe and turbulence measurements by linearized constant temperature hot-wire anemometry. A flexible slit along the acrylic test section allows probes to be introduced into the test section at any axial location. The sides of the slit are molded silicon rubber shaped to the inner contour of the test section. Pitot and hot-wire probes are mounted on a traversing mechanism that can locate the probes at any axial and radial position in a vertical plane containing the test section centerline; once a probe is in place, its yaw and pitch orientation can be adjusted continuously over 360 and ± 90 deg, respectively.

For the mean flow measurement, a 0.32-cm-diam directional five-hole pitot probe (United Sensor D.C. 125) is used in the null mode, where the probe is aligned in yaw and pitch by equalizing pressures in appropriate pairs of pressure taps. Axial and tangential velocities can be determined accurately. However, radial pressure gradients in swirling flow cause the pitch angle and radial velocity measurements to be uncertain; thus they are not reported here. High velocity gradients and high turbulence levels also contribute to uncertainty in axial and tangential velocity measurements. In the present experiments, regions with high turbulence are also regions with large radial gradients of velocity and pressure. To assess measurement accuracy, average speeds measured by hot-wire and pitot probe are compared. In regions of large gradients, whenever hot-wire results are valid (where local fluctuation levels are less than 30 to 40%), agreement within $\pm 10\%$ is obtained. Agreement between the two methods is better, about $\pm 2\%$, in regions where turbulence levels are low and gradients are not severe.

A commercial (Thermosystems) constant temperature anemometer unit and linearizer are used for hot-wire measurements; the sensor is a single 4-μ tungsten wire with a length-to-diameter ratio of about 320. The hot wire is operated at 250°C, which corresponds to an overheat ratio of 1.75. The hot wire is oriented normal to the flow; the yaw angle of the wire is that determined by the pitot probe. Mean speeds are obtained by averaging the linearized signal; values stable within $\pm 0.5\%$ can be obtained with nominal averaging times of 10 s.

Velocity fluctuation levels are determined from the linearized output with an rms meter. Detailed discussions of errors in fluctuation level measurements of this type may be found in Refs. 6 and 7. Errors result from high turbulence intensity, from three-dimensional wire response effects, and from temperature fluctuations in the flow. Of these, the largest source of uncertainty is high turbulence intensity because of the inherent inability of a single hot-wire sensor to resolve flow reversal. Therefore errors are largest in regions of high intensity. An error analysis[7] for measurements of turbulence intensity shows that errors will exceed 10% when the intensity exceeds 20-30%. Above this intensity range, the error increases rapidly with increasing intensity and is sen-

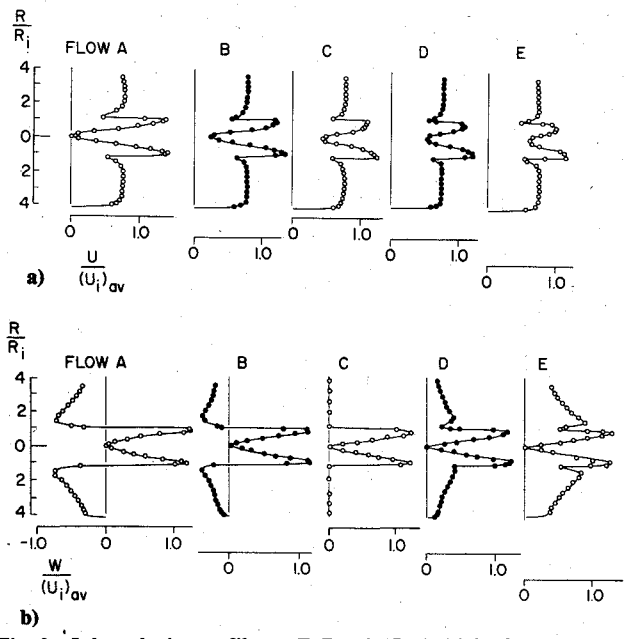

Fig. 2 Inlet velocity profiles at $Z/R_i = 0.17$; a) axial velocity, b) swirl velocity. Flow conditions given in Table 1.

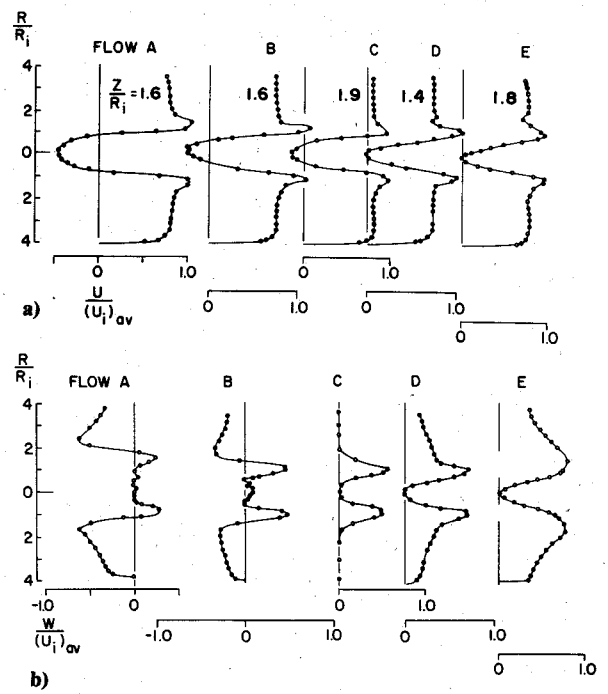

Fig. 3 Velocity profiles across the recirculation zone; a) axial velocity, b) swirl velocity. Flow conditions given in Table 1.

Table 1 Flow parameters, first experimental phase

Flow	$\frac{(U_o)_{av}}{(U_i)_{av}}$	$(U_i)_{av}$, m/s	S_i	S_o
A	0.69	42.5	0.59	−0.38
B	0.68	43.2	0.63	−0.19
C	0.74	41.0	0.68	0.0
D	0.70	42.5	0.69	0.21
E	0.70	41.7	0.71	0.42

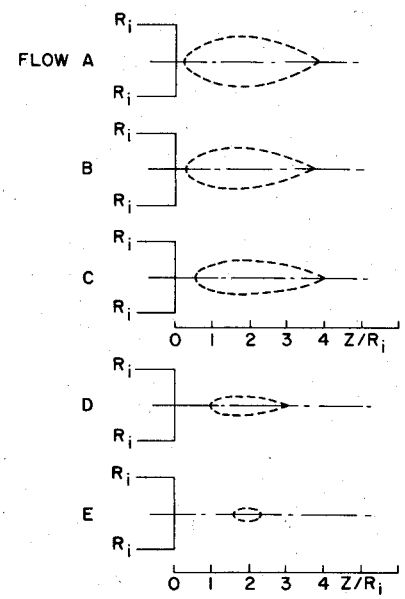

Fig. 4 Approximate reverse flow regions. Flow conditions given in Table 1.

sitive to anisotropy in turbulent velocity fluctuations. Thus, for turbulence intensities above 30%, only crude estimates of measurement error in intensity data are possible, and the results from hot-wire measurements should be used with caution. The following list gives estimated errors based on Ref. 7 for measured rms signals: At large radius and in downstream regions of the test section less than ±5% error is expected; for the interjet mixing region about ±5% to ±20% error is expected owing to higher turbulence intensity and temperature fluctuations; for the centerline regions, where local turbulence intensities are higher than 30% to 40%, ±20% to ±50% errors are expected.

Dissipation rate data are obtained by analog time differentiation. As discussed in Sec. III, various approximations and assumptions are made, and the dissipation results are only qualitative. Analog linearized hot-wire signals from several positons in the test section are recorded on an FM instrumentation tape recorder. The recorded signals are then digitized and processed on a minicomputer (Digital Equipment Corporation) to obtain the power spectrum of the fluctuating velocity component parallel to the mean velocity.

Procedure

For the first phase of the research, mean flow measurements by pitot probe are obtained for five flow conditions. The swirler for the inner jet is positioned 15.2 cm from the jet exit. Visual determination of the presence of reverse flow is made using a small wool tuft. The backflow regions determined by the tuft coincide roughly with the backflow regions determined by pitot probe measurement. Each radial traverse with the pitot probe requires between 4 and 5 h, and several days are required to complete the study of one flow condition. Before each traverse, the flow at the inlet plane (inner jet exit) is checked at two radial positions, one for the inner jet and one for the outer jet. The kinetic pressures at these points are reproducible to within ±1%.

Volume flow rates at different axial stations, obtained by integrating the axial velocity across the test section, agree to within ±2% for each flow condition.

During the second phase of experimentation, both pitot probe and hot-wire measurements are performed for one coswirl and one counterswirl flow condition. The swirler is positioned 12.2 cm upstream of the inner jet exit. Mean flows are measured by pitot probe, and hot-wire data are obtained at each point with the sensor aligned perpendicular to the local mean velocity. Mean velocities, rms fluctuations, dissipation rates, and power spectra are obtained as described. Fluid temperatures necessary for correcting hot-wire data are measured by thermocouple.

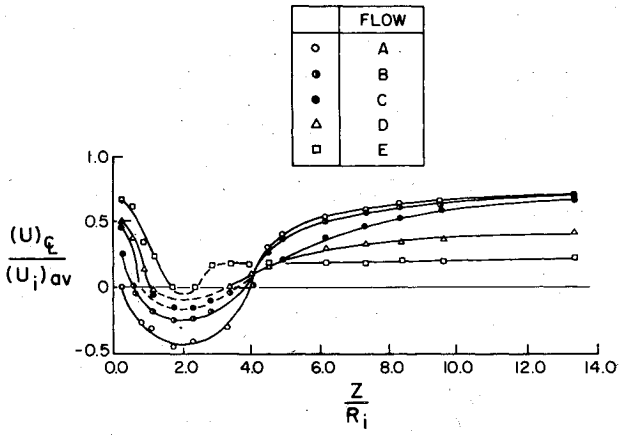

Fig. 5 Centerline axial velocity profiles. Flow conditions given in Table 1.

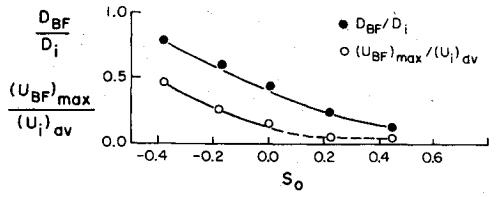

Fig. 6 Diameter of reverse flow region and magnitude of maximum reverse flow velocity. Flow conditions given in Table 1.

Table 2 Flow parameters, second experimental phase

Flow	$\frac{(U_o)_{av}}{(U_i)_{av}}$	$(U_i)_{av}$, m/s	S_i	S_o
F	0.68	29.6	0.58	0.54
G	0.67	30.3	0.49	−0.51

In presenting the results, the point on the centerline at the exit of the inner jet is defined as the origin. Radial and axial positions are normalized to the inner tube radius; velocities are normalized to the bulk average axial velocity of the inner jet.

III. Results

Effect of Outer Swirl on the Recirculation Zone

Mean velocity traverses are obtained for five flow conditions in order to study the effect of outer swirl on the recirculation zone. The outer swirl parameter S_o is varied from a maximum coswirl condition of $S_o = 0.42$ to a maximum counterswirl condition of $S_o = -0.38$. The ratio of the average axial velocity of the outer jet to the average axial velocity of the inner jet is approximately 0.7. A complete list of the flow parameters is given in Table 1; and the inlet profiles, obtained at 0.3 cm downstream of the inner jet exit, are shown in Fig. 2. Outside of the two boundary layers, the inlet axial velocities of the outer jet are roughly uniform, and the swirl velocities can be approximated by a free vortex profile. The outer swirl parameter S_o given in Table 1 is computed by integrating the velocity profiles across the outer annulus according to Eq. (1).

At the inlet, the inner jet is approximately under solid body rotation with a maximum swirl velocity of about 55 m/s. The axial velocity profiles have a minimum at the centerline. The inlet axial centerline velocity decreases as the outer swirl is changed from the maximum coswirl condition of $S_o = 0.42$ to the maximum counterswirl condition of $S_o = -0.38$. Also S_i changes from 0.71 to 0.59 as the outer swirl varies from $S_o = 0.42$ to -0.38.

For all five flow conditions considered, flow recirculation zones (or recirculation bubbles) are observed. Radial profile data of axial and tangential velocities for the cross section of maximum backflow are presented in Fig. 3; the approximate backflow regions are shown in Fig. 4. For the maximum coswirl condition the backflow region is quite small with the front stagnation point about 0.8 D_i from the inlet. With lower coswirl and then increasing counterswirl, the front stagnation point moves upstream and is positioned approximately at the inlet for the maximum counterswirl condition of $S_o = -0.38$.

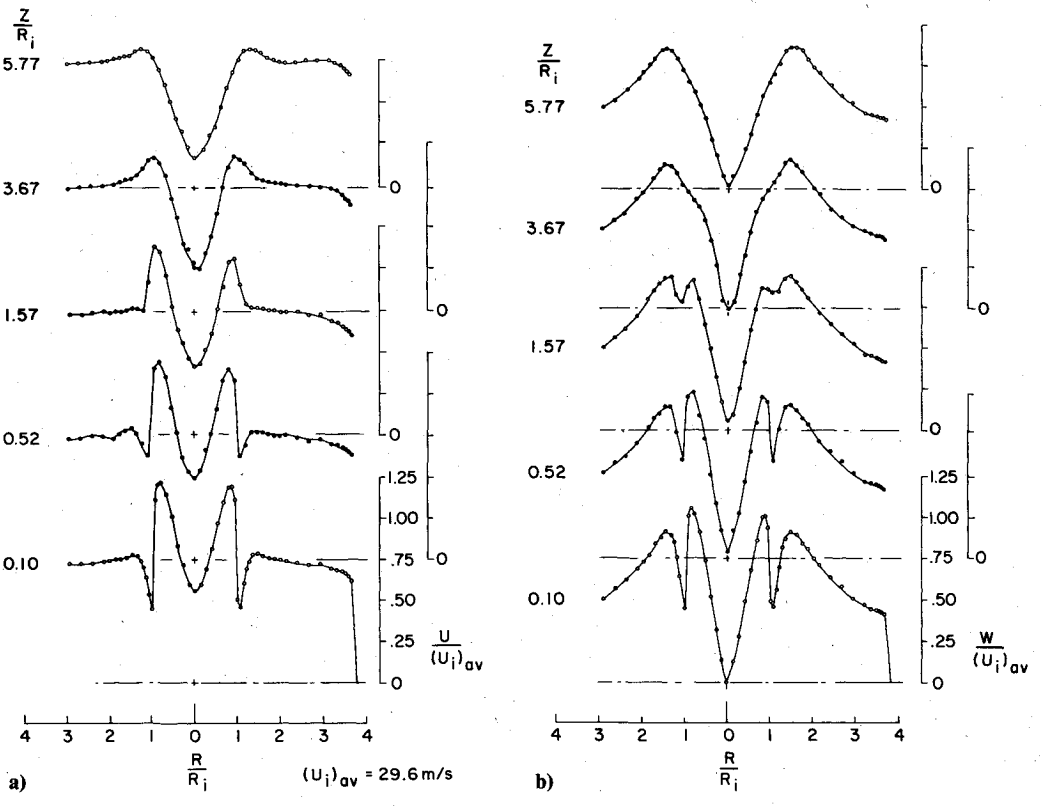

Fig. 7 Velocity profiles for coswirl condition; a) axial velocity, b) swirl velocity. Flow conditions given in Table 2.

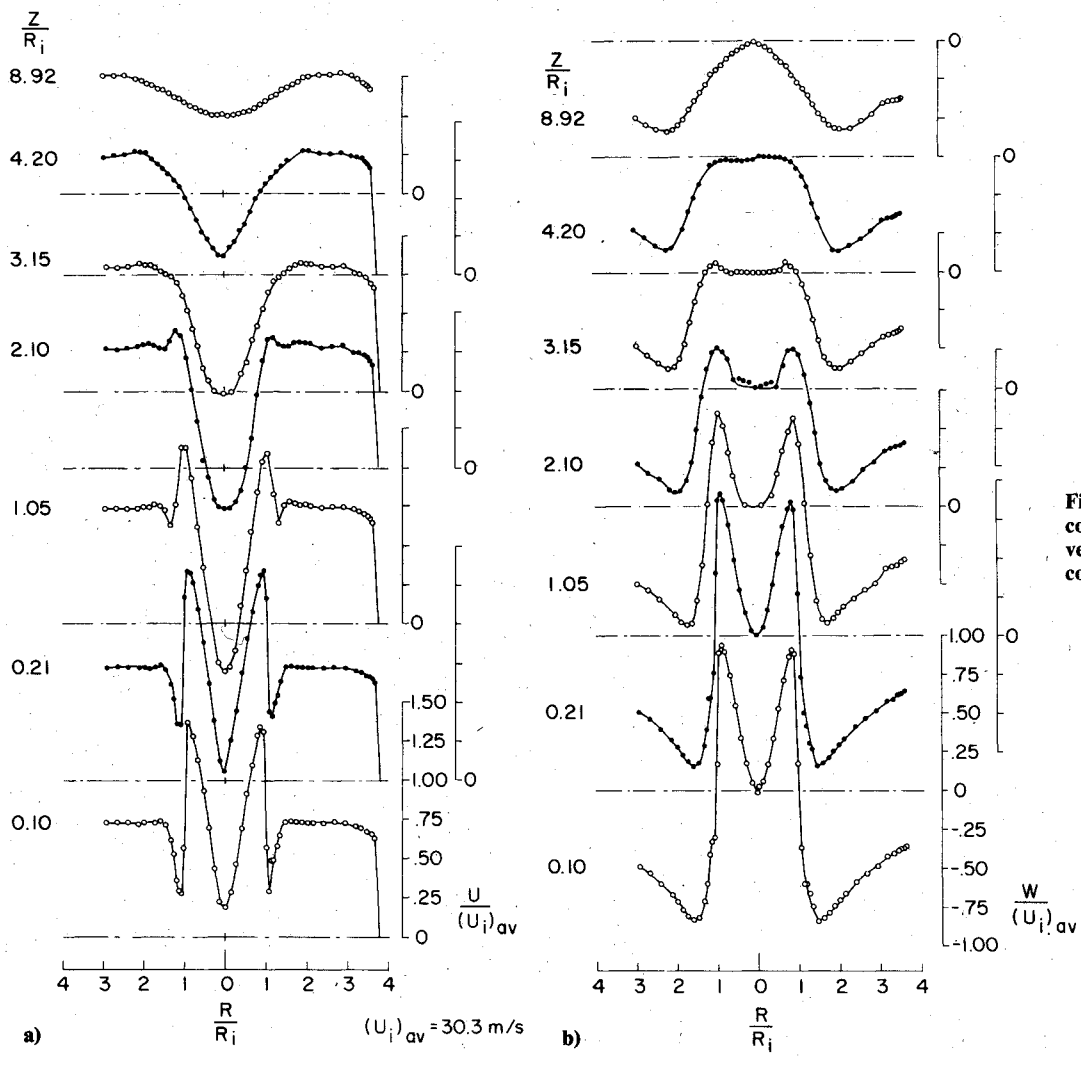

Fig. 8 Velocity profiles for counterswirl condition; a) axial velocity, b) swirl velocity. Flow conditions given in Table 2.

The maximum diameter of the backflow region and the magnitude of the maximum backflow velocity on the centerline increase as the outer swirl parameter S_o decreases from positive to negative values (Fig. 6). The centerline axial velocities are presented in Fig. 5. From Figs. 3 and 5 it can be seen that the recirculation zone appears to be a self-contained torroidal vortex with a front and a rear stagnation point on the centerline. Downstream of the recirculation zone, the centerline axial velocity recovers its positive value; the velocity recovers to higher values with counterswirl and no outer swirl than with coswirl. Under the maximum coswirl condition a center core of low axial velocity persists behind the recirculation zone.

It can be seen from Fig. 3 that, as the outer swirl changes from coswirl to counterswirl, turbulent diffusion and dissipation of the inner swirl drastically increase due to higher shear in the interjet shear layer. For maximum counterswirl, only a small vestige of the inner swirl is observed, even at small axial distances from the inlet. Due to the increasing diffusion and dissipation of the inner swirl as S_o decreases (from positive values to negative values) the axial pressure gradient becomes more adverse, leading to a larger recirculation bubble and a larger back flow velocity.

Mean Flow Results for a Coswirl and a Counterswirl Flow

Detailed velocity and pressure traverses are obtained for two flow conditions with the inner swirler positioned 12.2 cm upstream of the inlet. The swirl parameters are $S_i = 0.49$, $S_o = -0.51$ for counterswirl, and $S_i = 0.58$, $S_o = 0.54$ for coswirl. The flow parameters are given in Table 2. Figures 7-10 show the development in the axial direction of the axial and tangential velocities and the pressure for both cases.

Again, at the inlet, the outer swirl is approximately free vortex outside the boundary layers, and the inner swirl is approximately solid body rotation. The axial velocity for the outer jet is almost uniform across the annulus at the inlet, with slightly higher values at smaller radial distances. The total head for the outer jet (with $R/R_i > 1.8$) is found to be independent within a few millimeters of water of radial position; this approximate constancy leads to the axial velocity profiles observed.

Downstream of the inlet, coswirl and counterswirl flows show quite different axial development. For coswirl, gradual changes in axial direction can be seen in Figs. 7 and 8. Axial velocities in the central region of the flow diminish to low values but no flow reversal is observed. In the interjet mixing layer turbulent diffusion smooths out gradients in both axial and tangential velocity in a relatively short axial distance. At the inlet outside the boundary layers, swirl velocities in both jets are almost matched near the inner tube wall (Fig. 7). As turbulent diffusion smooths out the swirl defect due to the wall boundary layers, the swirl profile approximates the Burgers vortex,

$$W = K\frac{R_o}{R}\left(1 - \exp\left[-\alpha\frac{R^2}{R_o^2}\right]\right) \qquad (2)$$

with $K \simeq 12.5$ m/s and $\alpha \simeq 8.5$ at $Z/R_i = 5.77$. The Burgers vortex is an exact solution for a viscous flow with streamwise vorticity produced by radial inflow with irrotational flow at large radial distance.[8] Single swirling flows with radial inflow are usually observed to attain the Burgers swirl profile.[9-11]

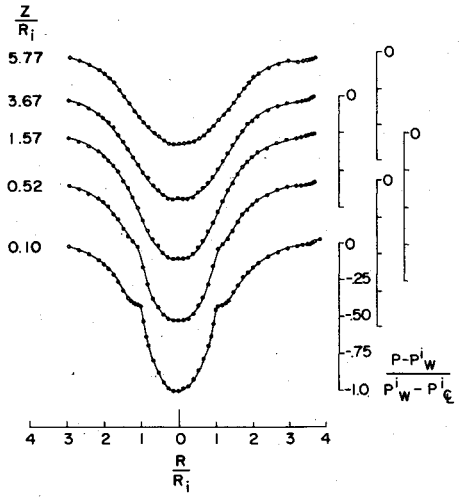

Fig. 9 Static pressure profiles for coswirl condition. $P^i_w = -5.6$ cm water, gage; $P^i_w - P^i_{\text{℄}} = 14.8$ cm water. Flow conditions given in Table 2.

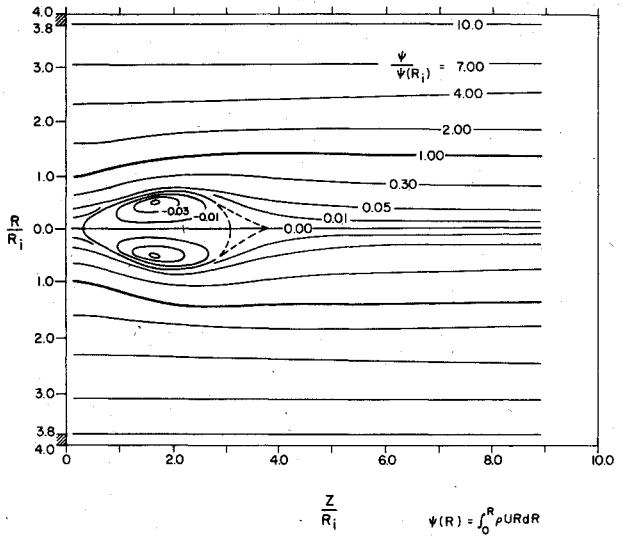

Fig. 11 Stream function contours for counterswirl condition. Flow conditions given in Table 2.

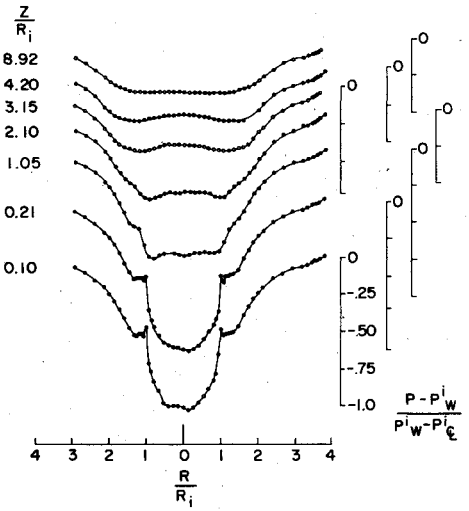

Fig. 10 Static pressure profiles for counterswirl condition. $P^i_w = -5.6$ cm water, gage; $P^i_w - P^i_{\text{℄}} = 8.9$ cm water. Flow conditions given in Table 2.

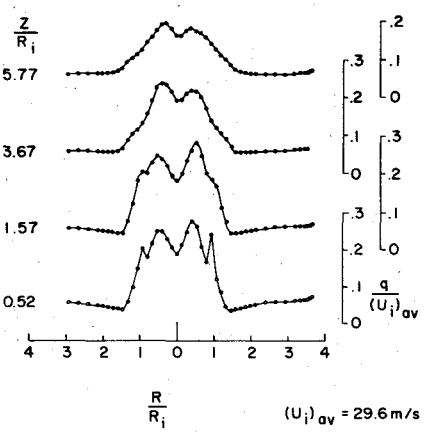

Fig. 12 Normalized fluctuating velocity intensity for coswirl condition. Flow conditions given in Table 2.

With two coswirling jets in the present experiment, attainment of a Burgers swirl profile can be seen as a consequence of swirl matching at the inlet. Owing to this matching, the inner swirl can be thought of as replacing the swirl of the viscous core of a single swirling flow with radial inlet. The Burgers profile is reached as diffusion in the inner-jet region obliterates the swirl defect of the boundary layers on the wall of the inner tube.

Figures 9 and 10 show rapid flowfield development in the axial direction under the counterswirl condition. Large deceleration in the axial flow of the inner jet leads to a self-contained torroidal vortex bubble with a small recirculating flow rate, about 5% of the inner jet flow rate (Fig. 11). Very low swirl velocities are measured inside the bubble, which also is characteristic of the five flows presented in the last section (Fig. 3). As the vortex core of the inner jet cannot convectively penetrate the self-contained bubble, swirl can only be transferred to the bubble by turbulent diffusion. Thus only low swirl is observed in the bubble. The observation of low tangential velocity in the recirculation zones is consistent with other measurements in bubble form vortex breakdowns.[10] Measurements by Syred, Chigier, and Beér in a swirling jet issuing into stagnant air,[12] however, show high swirl velocities in the recirculation bubble, as if the vortex core could traverse through the bubble; this is probably due to large turbulent transport coupled with large mean velocity gradients.

Flow deceleration and formation of the recirculation bubble is affected significantly by the large adverse pressure gradient exerted on the inner jet (Fig. 10). This adverse pressure gradient is caused by dissipation and diffusion of swirl and also by flow divergence. Upstream of the bubble we can use the cylindrical approximation[1]

$$\frac{\partial P}{\partial R} \simeq \rho \frac{W^2}{r} \tag{3}$$

With $(\partial P/\partial Z)_{R=R_o} \simeq 0$ as measured, Eq. (3) leads to

$$\left(\frac{\partial P}{\partial Z}\right)_{R=0} \simeq -2\int_0^{R_o} \rho \frac{|W|}{R} \frac{\partial |W|}{\partial Z}\, dR \tag{4}$$

In a counterswirl flow, diffusion and dissipation of the swirl in the interjet shear layer cause large negative values of $\partial |W|/\partial Z$, leading to a strong adverse pressure gradient.

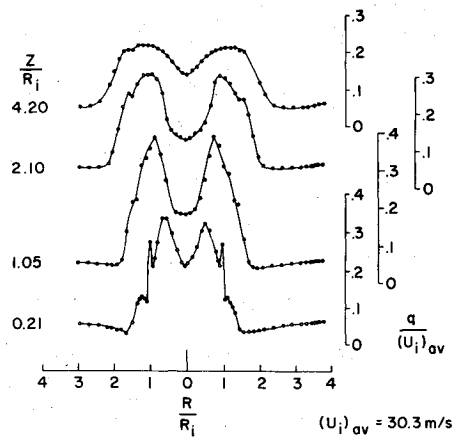

Fig. 13 Normalized fluctuating velocity intensity for counterswirl condition. Flow conditions given in Table 2.

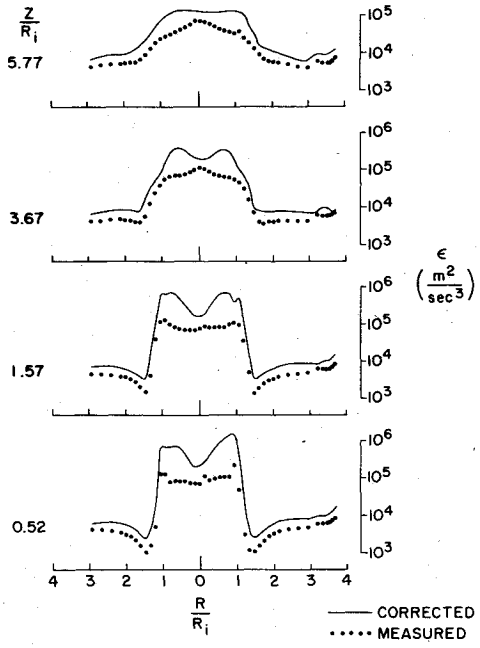

Fig. 14 Energy dissipation rate for coswirl condition. Flow conditions given in Table 2.

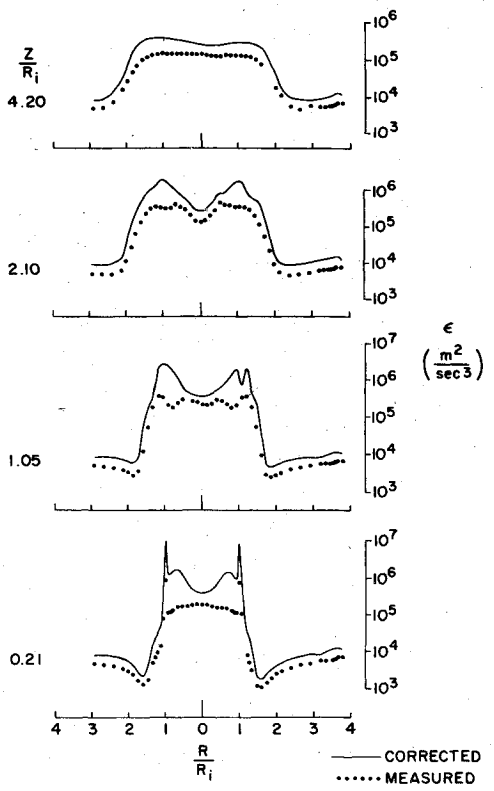

Fig. 15 Energy dissipation rate for counterswirl condition. Flow conditions given in Table 2.

Stronger counterswirl leads to larger adverse pressure gradients and larger recirculation bubbles. Also it can be seen that flow expansion at the inlet further increases the adverse pressure gradient.[1]

It is suggested that the recirculating flows observed here belong to the vortex breakdown family. The external boundaries of the recirculation bubbles observed in this experiment are quite similar to the boundaries of axisymmetric or bubble vortex breakdowns in laminar flows.[10] However, the double-cell internal structure of the laminar axisymmetric form noted by Faler and Leibovich[10] is not observed here or in other turbulent swirling flows (see Ref. 13). Also, no stagnation point downstream of the bubble is observed, while in laminar vortex breakdown a stagnation point leading to a spiral breakdown may follow the axisymmetric breakdown.[9] Grabowski and Berger[14] suggest that the spiral breakdown downstream of an axisymmetric breakdown may be due to inertial effects in the radial inflow closing behind the bubble. Inertia causes the inward flowing fluid to overshoot the equilibrium position between the pressure gradient and centripetal acceleration; subsequently, fluid can move outward, forming the second spiral vortex breakdown. In turbulent flows, strong diffusion and dissipation may act against this inertial effect to prevent the formation of a spiral breakdown.

In laminar vortex breakdown, the position and form of the breakdown are quite sensitive to disturbances by probes of the flowfield. Turbulent recirculation bubbles observed here and in a similar flow configuration[3-5] apparently are not sensitive to probe disturbances. While cylindrical sampling probes in combusting flow are observed to cause perturbations at certain locations,[5] there is no evidence that thermocouples, hot-wire, or pitot probes induce perturbations in any of our flows.[5,6] A review[15] of the literature on turbulent swirling flow measurements indicates that disturbances are not observed when small probes (small compared to the diameter of the vortex core) are used in turbulent flow.

Faler and Leibovich[10] and Garg and Leibovich[11] observed highly periodic oscillations in laminar vortex breakdown flows. Periodic flow osicallations originating from the inner jet are observed in the present study. Data on these flow oscillations are presented and discussed in the latter part of the next section.

Hot-Wire Measurement

Figures 12-15 show fluctuation levels (rms values of the fluctuating velocity) and dissipation rates for the counterswirl and coswirl cases. The fluctuating velocity component parallel to the mean flow velocity is measured with the hot-wire sensor aligned perpendicular to the mean velocity as determined by pitot probe measurements.

In calculating the dissipation rate, the hypothesis of local isotropy and Taylor's hypothesis[16] are invoked to obtain an expression for the dissipation rate:

$$\epsilon \simeq 15\nu \frac{1}{Q^2}\left(\frac{\partial q'}{\partial t}\right)^2 \tag{5}$$

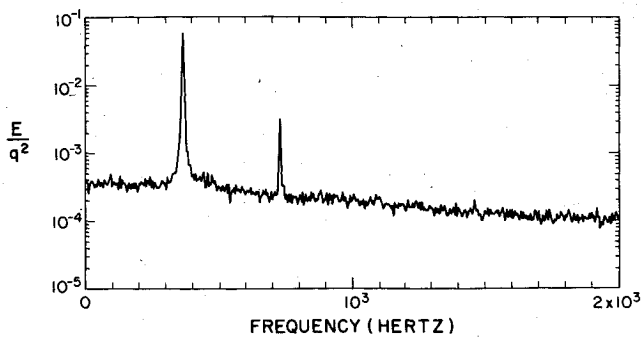

Fig. 16 Normalized power spectrum of fluctuating velocity q' for coswirl condition. Flow conditions given in Table 2.

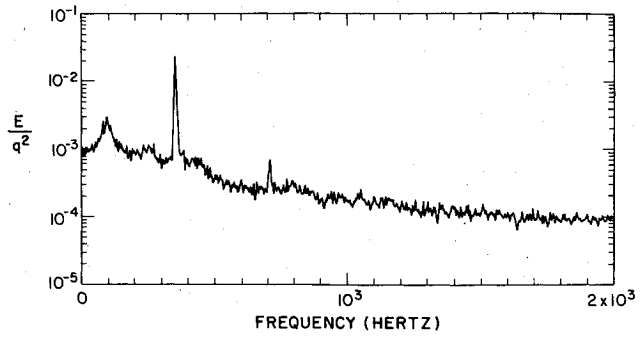

Fig. 17 Normalized power spectrum of fluctuating velocity q' for counterswirl condition. Flow conditions given in Table 2.

Estimates of the Kolmogorov length scale‡ indicate that it is much smaller than the hot-wire length, which leads to averaging over the hot-wire length and attenuation of the dissipation spectrum at high wave numbers.[17] Correction for this finite length effect is carried out according to the method given in Ref. 17. The turbulent dissipation also occurs at very high frequencies (k_d is translated into f_d under Taylor's hypothesis; $f_d \simeq (Q/2\pi)k_d$), which are far beyond the hot-wire anomometer cutoff frequency of about 30 kHz. The anomometer therefore cannot measure the full dissipation rate, and the measured values are extrapolated to the full dissipation rate by assuming the theoretical turbulence spectrum of Pao.[18] The extrapolation method is explained in more detail in Ref. 6. Due to the errors involved in the wire length correction and frequency extrapolation, the results for ϵ are approximate and are considered only qualitative. Results from direct measurement and the corrected results for the dissipation rate are given in Figs. 14 and 15.

At the inlet axial station, fluctuation levels for the counterswirl and coswirl cases are similar (Figs 12 and 13). Normalized (to the bulk mean axial velocity of the inner jet) fluctuation levels for the outer jet outside the boundary layers are low (between 3 and 7%), and much higher fluctuation levels are found in the inlet region of the inner jet (between 20 and 30%).

In the outer jet, the fluctuations are random turbulence, as determined from frequency analysis. At the inlet between $R/R_i = 1.5$ and 3.7, the turbulence level increases with increasing radial position. Under the Rayleigh stability criterion,[19] fluid particles at smaller radial distances (in the range $1.5 \leq R/R_i < 3.7$) are found to be more stable than fluid particles at larger radial distances. This is a consequence of the slight difference in the swirl velocity of the outer flow from a free vortex profile, $W = CR$, which results in an increasingly positive value of $\partial \mid RW \mid /\partial r$ as the radial distance decreases. The Rayleigh criterion says that disturbances are suppressed if $\partial \mid RW \mid /\partial r > 0$; it is therefore believed that the higher stability of fluid particles at smaller radial distance leads to stronger turbulence suppression there. A marked decrease in dissipation rates also occurs where turbulence is suppressed (Figs. 14 and 15).

At the inlet, the fluctuation levels of the inner jet are high, as mentioned earlier, and have unexpected profiles with off-centerline maxima at approximately $R/R_i = 0.5$. Frequency analyses of the fluctuating velocities in the inner jet show periodic oscillations uncharacteristic of random turbulence, and these maxima occur at positions where the periodic oscillations are strongest. The strength of these oscillations is lower on the centerline and near the inner tube wall. At the inlet, the energy of the strongest periodic fluctuations is about 30% of the total fluctuating energy for counterswirl and is about 40% for coswirl; typical power spectra are shown in Figs. 16 and 17. These spectra are obtained at the inlet at $R/R_i = 0.4$ and two harmonics can be easily observed. At other stations up to four harmonics are noted. The frequencies of the fundamental harmonics are 367 and 356 Hz for coswirl and counterswirl, respectively. These frequencies are comparable to the rotational frequencies of the inner flow, which are about 300 Hz for coswirl and 275 Hz for counterswirl.

The streamwise development of q is markedly different for coswirl than for counterswirl (Figs 12 and 13). Under coswirl, where interjet shear is small and the flow is nearly cylindrical, turbulence energy production and outward radial diffusion are not significant. Higher fluctuation levels are confined to the core, with $R/R_i < 1.5$. Fluctuation levels decay gradually in the streamwise direction for axial distances larger than one inner tube diameter. The periodic oscillations observed at the inlet pass downsteam with diminishing magnitudes but with unaltered frequencies and with little radial diffusion. The periodic fluctuations are only observed near the maxima in the radial profiles of the fluctuation level at $R/R_i = 0.5$.

Under the counterswirl condition, strong turbulence is produced in the shear layer between the two jets. The fluctuation levels inside the recirculation zone are low and are, in fact, smaller than the centerline fluctuation level at the inlet. Downstream of the recirculation zone, fluctuation levels are lower in the core flow ($R/R_i < 1$) than in the interjet shear layer. The periodic oscillations pass around the recirculation zone, and only weak oscillations can be observed inside the bubble.

For both flow conditions, regions of high q are also regions of high energy dissipation rates (Figs. 14 and 15). Dissipation rates in the central regions and in the interjet shear layers are much higher (two orders of magnitude) than dissipation rates in the outer jet. As noted earlier, since dissipation occurs at high wave numbers and at length scales much smaller than the length of the hot wire, results for dissipation rates are only approximate and should be considered only as qualitative indications of the actual dissipation rates.

Estimates of the different length scales of the flows can be obtained from measurements of fluctuation levels and dissipation rates.[16] The sizes of the energy-containing eddies can be approximated from dimensional analysis:

$$\ell \sim q^3/\epsilon \tag{6}$$

The Taylor microscale is obtained from the isotropic relation

$$\lambda \sim [15\nu(q^2/\epsilon)]^{1/2} \tag{7}$$

Finally, the Kolmogorov length scale, where most dissipation occurs, is given by

$$\eta = (\nu^3/\epsilon)^{1/4} \tag{8}$$

‡$\eta = (\nu^3/\epsilon)^{1/4}$, where ϵ is estimated by $\epsilon \sim q^3/\ell$ and ℓ is estimated by $q/\ell \sim \mid \partial Q/\partial r \mid$.

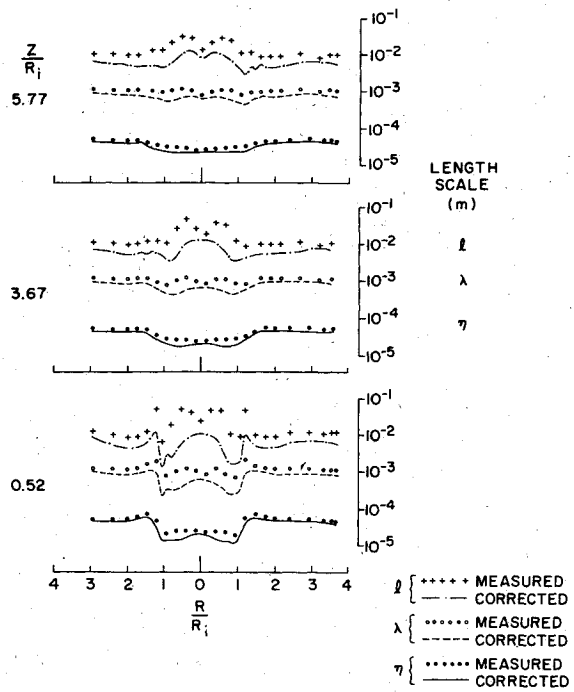

Fig. 18 Length scales for coswirl condition. Flow conditions given in Table 2.

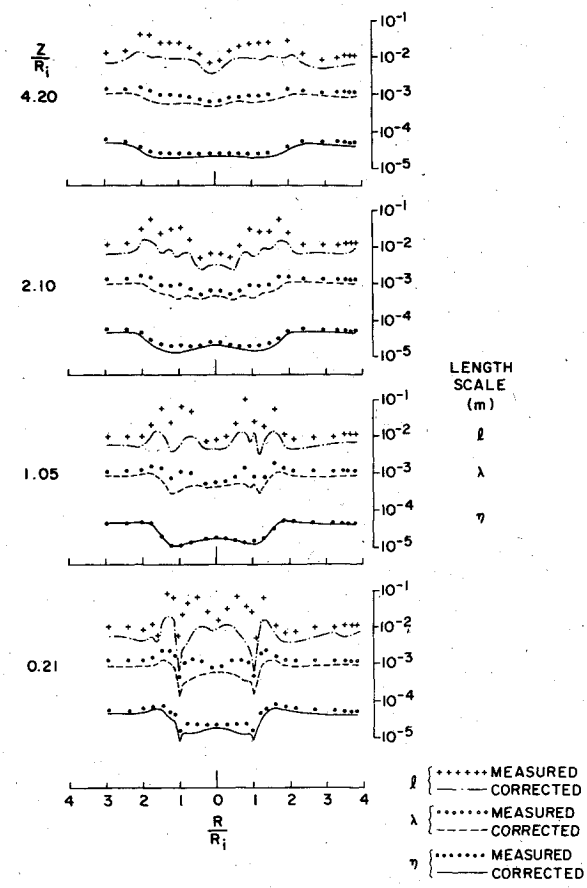

Fig. 19 Length scales for counterswirl condition. Flow conditions given in Table 2.

These scales are computed from the measured and extrapolated values of ϵ and typical results are shown in Figs. 18 and 19. ℓ is inversely proportional to ϵ; thus its value suffers as much uncertainty as the value for ϵ. There is less uncertainty in the result for λ and η since they are proportional to smaller powers ($-\frac{1}{2}$ and $-\frac{1}{4}$) of ϵ. It is seen that ℓ is on the order of 1 cm, which is about $\frac{1}{4}$ of the inner jet diameter. Trends in the streamwise development of ℓ cannot be detected, most likely because of uncertainty in its value. In the outer stream, λ and η have values of about 1 and 0.04 mm, respectively; it is seen that even in the outer flow the Kolmogorov length scales are extremely small. At the inlet, λ and η have very low values in the inner jet region, associated with the high dissipation rate there ($\lambda \sim 0.3$ mm and $\eta \sim 0.01$ mm). Further downstream, smaller λ and η are observed in the interjet mixing layer.

IV. Significance for Premixed Combustion

Combustion studies in a swirl combustor with two swirling jets have been performed[3-5] with the inner jet consisting of premixed fuel (methane) and air, and the outer jet consisting of secondary air. The results of these combustion studies can be correlated with the present fluid dynamical observations to arrive at a better understanding of the combustion process.

The importance of swirl on combustion lies in its effects on the recirculation zone and on turbulence properties. Due to these effects, the combustion under coswirl is significantly different from combustion under counterswirl conditions. Combustion observations for high counterswirl conditions[3-5,20] indicate a recirculation zone similar to that observed in the present experiment. Reactions are noted outside the recirculation zone, including the region upstream of the front stagnation point. With reduced counterswirl and increasing coswirl a hot luminous core extending downstream of the recirculation zone is observed. Observations do not support the stirred reactor concept and indicate that combustion is stabilized in the forward stagnation region of the recirculation zone.[20] In this case, the internal structure of the recirculation zone is of much less importance to the combustion process than are the turbulent transport properties in the vicinity of the recirculation zone and in the interjet shear layer. Flame stability is dependent on the local conditions in the inner jet near the front stagnation point. Downstream of this stagnation point the turbulence levels and the transport properties in the interjet shear layer will largely determine the combustion process. Under counterswirl conditions, as can be seen from the high turbulence generation in the interjet shear layer, turbulent mixing is highly vigorous and thus reaction is quenched in the interjet shear layer. Under coswirl conditions, since the interjet mixing is not as strong, a long hot core of gas extends from the front stagnation point and reactions persist farther downstream, leading to more efficient combustion and pollutant concentrations different from those under counterswirl conditions.[4,5]

Periodic flow oscillations in swirl combustors may have an effect on flame stabilization upstream of the front stagnation point and influence mixing through their resultant Reynolds stresses. The oscillations observed in this experiment may be related to the processing vortex core (PVC) described by Syred and Beér.[13] Similar oscillations are observed in vortex breakdown flowfields.[10,11] The oscillations in laminar vortex breakdown flows correspond closely to theoretical predictions of the linearly most unstable normal modes of the time-average mean flow profiles.[11] For the present swirling flows, an extensive study of flow oscillations also indicates that these oscillations can be related to the most unstable asymmetrical waves.[6]

In addition to the coherent fluctuations observed, two other distinct types of oscillations have been noted under combusting conditions. First, in confined combustion chambers, oscillations with frequencies closely corresponding to the acoustic resonance frequencies of the chamber have been reported.[21] Second, low frequency axial oscillations (a few Hertz) of the recirculation zone and the combustion region have been noted.[3-5,20] The mechanisms for this low frequency oscillation are unclear, but we speculate that it may be caused by an unstable interaction between combustion and swirl.

With combustion, the values of S_i may oscillate: Combustion near the inlet accelerates the flow axially, which reduces S_i and moves the stagnation point downstream; as the flame front moves downstream, fluid near the inlet cools and S_i increases, causing the stagnation point to move upstream. The process may repeat, resulting in the low frequency oscillations of the recirculation zone observed. In summary, we suggest that periodic and low frequency oscillations in swirl combustors may be caused by three distinct mechanisms: 1) fluid dynamic instability, 2) acoustic resonance, and 3) thermofluid dynamic instability. These mechanisms and possibly others need more detailed investigation and should be incorporated in the study of combustion processes in swirling flows.

V. Summary

Extensive measurements of mean flow, turbulence characteristics, and flow oscillations are obtained in a model swirl combustor under noncombusting conditions. The significance of the measurement results for combustion processes in such a combustor is discussed.

It is seen that in this coaxial swirling jet combustor, the outer swirl has a strong effect on the formation of a recirculation zone and on mixing characteristics in the interjet shear layer. Except under one coswirl flow, single cell, torroidal recirculation zones are observed on the centerline near the inner jet exit. As the outer swirl magnitude is first decreased from maximum counterswirl to zero and then increased to give coswirl, the size and the reverse flow velocities in the recirculation bubble diminish. Tangential velocities inside the bubble are low. High levels of turbulent fluctuations and large dissipation rates characterize the central flow region for both coswirl and counterswirl conditions, while the outer flow regions exhibit relatively low turbulence levels. More turbulence is generated in the interjet shear layer under counterswirl than for coswirl.

The importance of swirl on combustion for the special case of premixed reactants lies in the formation of a front stagnation region that helps stabilize the flame, and in its influence on the mixing process near the boundary of the recirculation zone where most reaction occurs. Observations in combusting conditions[3-5,20] do not support the concept of well-stirred reactors. Rapid mixing in the interjet shear layer under counterswirl conditions will quench reaction, causing low efficiency and high emissions of carbon monoxide and hydrocarbons.

In the present experiment, periodic flow oscillations are observed and contribute significantly to the high fluctuation levels in the central regions of the flow. The oscillations originate from the inner jet, pass downstream, and mostly bypass the recirculation zone. These oscillations may have a significant influence on flame stability and also on the mixing process in the interjet shear layer. It is suggested that these oscillations derive their energy from fluid dynamic instability. Other types of oscillations in swirl combustors may exist, and it appears that three distinct mechanisms can cause oscillations in swirl combustors: fluid dynamic instability, acoustic resonance, and unstable interaction between combustion and swirl.

Acknowledgment

This research was partially supported by NSF-RANN, Grant No. GI-36538, and the NASA Lewis Research Center, Grant No. NSG-3019.

References

[1] Hall, M. G., "Vortex Breakdown," *Annual Review of Fluid Mechanics,* Vol. 4, 1972, pp. 195-218.

[2] Leibovich, S., "The Structure of Vortex Breakdown," *Annual Review of Fluid Mechanics,* Vol. 10, 1978, pp. 221-246.

[3] Martin, D. T., Gouldin, F. C., and Yetter, R. A., "Preliminary Evaluation of a Vortex Breakdown Stabilized Combustor," Cornell University, Ithaca, N. Y., College of Engineering Energy Program, Rept. EPR-75-9, Nov. 1975.

[4] Yetter, R. A. and Gouldin, F. C., "Exhaust Gas Emissions of a Vortex Breakdown Stabilized Combustor," Cornell University, Ithaca, N. Y., College of Engineering Energy Program Rept. EPR-77-3, 1977.

[5] Oven, M. J., Gouldin, F. C., and McLean, W. J., "Temperature and Species Concentration Measurements in a Swirl Stabilized Combustor," *17th Symposium (International) on Combustion,* The Combustion Institute, Pittsburgh, Pa., 1979, pp. 363-374.

[6] Vu, B. T., "Experiments on Turbulent Co-axial Swirling Flows," Ph.D. thesis, Cornell University, Ithaca, N. Y., (in preparation).

[7] Bradbury, L. J. S., "Measurements with a Pulsed-Wire and a Hot-Wire Anemometer in the Highly Turbulent Wake of a Flat Plate," *Journal of Fluid Mechanics,* Vol. 77, 1976, pp. 473-497.

[8] Burgers, J. M., "A Mathematical Model Illustrating the Theory of Turbulence," *Advances in Applied Mechanics,* Vol. 1, Academic Press, New York, 1948, p. 198.

[9] Faler, J. H. and Leibovich, S., "Disrupted States of Vortex Flow and Vortex Breakdown," *Physics of Fluids,* Vol. 20, 1977, pp. 1385-1400.

[10] Faler, J. H. and Leibovich, S., "An Experimental Map of the Internal Structure of a Vortex Breakdown," *Journal of Fluid Mechanics,* Vol. 86, 1978, p. 313.

[11] Garg, A. K. and Leibovich, S., "Spectral Characteristic of Vortex Breakdown Flow Fields," *Physics of Fluids,* Vol. 22, 1979, pp. 2053-2064.

[12] Syred, N., Chigier, N. A., and Beér, J. M., "Flame Stabilization in Recirculation Zones of Jets with Swirl," *13th Symposium (International) on Combustion,* The Combustion Institute, Pittsburgh, Pa., 1971, pp. 612-624.

[13] Syred, N. and Beér, J. M., "Combustion in Swirling Flows: A Review," *Combustion and Flame,* Vol. 23, 1974, pp. 143-201.

[14] Grabowski, W. J. and Berger, S. A., "Solution of the Navier-Stokes Equations for Vortex Breakdown," *Journal of Fluid Mechanics,* Vol. 75, 1975, pp. 525-544.

[15] Gouldin, F. C., "Probe Measurements in Multi-Dimensional Reacting Flow," *Testing and Measurement Techniques in Heat Transfer and Combustion,* AGARD, Neuilly Sur Seine, France, CP-281, Sept. 1980.

[16] Tennekes, H. and Lumley, J. L., *A First Course in Turbulence,* M.I.T. Press, Cambridge, Mass., 1972.

[17] Wyngaard, J. C., "Measurement of Small-Scale Turbulence Structure with Hot Wires," *Journal of Physics E,* Ser. 2, Vol. 1, 1968, pp. 1105-1108.

[18] Pao, Y. H., "Structure of Turbulent Velocity and Scalar Fields at Large Wave Numbers," *Physics of Fluids,* Vol. 8, 1965, pp. 1063-1075.

[19] Rayleigh, J. W. S., "On the Dynamics of Revolving Fluids," *Proceedings of the Royal Society of London, Ser. A,* Vol. 6, 1916, p. 148.

[20] Beyler, C. L. and Gouldin, F. C., "Flame Structure in a Swirl Stabilized Combustor Inferred by Radiant Emission Measurements," *18th Symposium (International) on Combustion,* The Combustion Institute, Pittsburgh, Pa., 1981, pp. 1011-1019.

[21] Spadaccini, L. J., Owen, F. K., and Bowman, C. T., "Influence of Aerodynamic Phenomena on Pollutant Formation in Combustion (Phase I. Gaseous Fuels)," Environmental Protection Agency, Washington, D. C., EPA 600/2-76-247a, Sept. 1976.